A Soluble Oligomer of Tau Associated with Fiber Formation Analyzed by NMR

Dylan W. Peterson,[‡] Hongjun Zhou,[§] Frederick W. Dahlquist,[‡,§] and John Lew*[,‡]

Department of Molecular, Cellular and Developmental Biology and Department of Chemistry, University of California, Santa Barbara, Santa Barbara, California 93106

Received December 18, 2007; Revised Manuscript Received May 9, 2008

ABSTRACT: Alzheimer's disease (AD) is characterized by the intracellular accumulation of the neurofibrillary tangles comprised mainly of the microtubule-associated protein, tau. A critical aspect of understanding tangle formation is to understand the transition of soluble monomeric tau into mature fibrils by characterizing the structure of intermediates along the aggregation pathway. We have carried out multidimensional NMR studies on a C-terminal fragment of human tau (tau^{187}) to gain structural insight into the aggregation process. To specifically monitor intermolecular interaction between tau molecules in solution, we combined ^{15}N- and ^{14}N-labeled tau, the latter of which was modified with a paramagnetic nitroxide spin label (MTSL). Paramagnetic relaxation enhancement (PRE) of ^{15}N-tau by interaction with MTSL-^{14}N-tau allowed identification of low molecular weight oligomers of tau^{187} that formed in response to heparin-induced aggregation. Two regions, VQIINK^{280} and VQIVYK^{311}, were exclusively broadened by MTSL located at varied positions in the tau molecule. We propose that soluble oligomers of tau^{187} are generated via intermolecular interactions at these motifs triggered by heparin addition. However, the associated line broadening at these motifs cannot be due to interaction between tau^{187} and heparin directly. Instead, these specific interactions necessarily occur between tau molecules and are intermolecular in nature. Our data support the idea that VQIINK^{280} and VQIVYK^{311} are the major, if not sole, critical regions that directly mediate intermolecular contact between tau molecules during the early phases of aggregation.

The progression of Alzheimer's disease (AD)[1] correlates most closely with appearance of the neurofibrillary tangles, insoluble intracellular fibers of paired helical filaments (PHF) arising from the misfolding and aggregation of the neuronal-specific microtubule-associated protein, tau (*1–3*). As a result, it is expected that an understanding of the mechanism of tau aggregation in detail will be key to our understanding of the molecular basis of Alzheimer's disease and the possible discovery of therapeutics.

Tau is critical for the regulation of microtubule dynamics in normal neurons (*3–5*). In humans, six isoforms of tau (ranging from 352 to 441 amino acids) are expressed via alternative splicing of a single gene, all six isoforms being present in the tangles in AD (*6*). The isoforms of tau share in common an acidic amino-terminal region, a central proline-rich domain, and a basic carboxyl terminus, the latter of which contains three or four imperfect repeat sequences that together constitute the microtubule binding domain (MTBD) (*7, 8*). A crucial advance in the field has been the ability to express wild-type as well as genetically engineered forms of human tau by recombinant methods. Purified, recombinant tau can self-aggregate to form fibrils that are highly similar if not identical to filaments isolated from AD brain (*9*). Using this assay, the structural determinants essential for aggregation and fibril formation have been identified. The key determinants for aggregation lie within the MTBD, and fibers can be generated from short truncation fragments of tau containing these determinants (*9, 10*).

Monomeric tau from recombinant sources has been well characterized at the biochemical level (*11*), and studies characterizing the secondary structure content of tau fibrils have been conducted (*12–14*). Tau free in solution is best described as an unfolded, highly flexible "random coil" under native conditions based on CD and FTIR spectroscopic data, hydrodynamic studies, and NMR studies of selected tau peptides (*15–19*). On the other hand, tau fibrils display significant secondary structure, most studies reporting predominant β-sheet or cross-β-sheet structure in fibers generated from recombinant tau or PHF-tau isolated from brain (*12–14, 20, 21*).

In contrast, little is known about the mechanism by which tau undergoes self-aggregation to form mature fibrils. In particular, the kinetics of intermediate species and their structural characterization are not known. Recently, it has been shown that soluble intermediates, as opposed to the fibers themselves, may be the key to cell death associated with tau aggregation (*22*). Thus the importance of characterizing the relevant intermediates in the aggregation pathway becomes of even greater urgency in our understanding of the mechanism of neurodegeneration and the potential development of therapeutics.

* Address correspondence to this author. Tel: (805) 893-5336. Fax: (805) 893-4724. E-mail: lew@lifesci.ucsb.edu.

[‡] Department of Molecular, Cellular and Developmental Biology, University of California, Santa Barbara.

[§] Department of Chemistry, University of California, Santa Barbara.

[1] Abbreviations: AD, Alzheimer's disease; MTSL, (1-oxyl-2,2,5,5-tetramethylpyrrolidin-3-yl)methyl methanethiosulfonate; Para, paramagnetic; PRE, paramagnetic relaxation enhancement; Dia, diamagnetic; SL, spin label; MTBD, microtubule binding domain; PHF, paired helical filament; TMAO, trimethylamine oxide; NOE, nuclear Overhauser effect; NMR, nuclear magnetic resonance; DTT, dithiothreitol; CSI, chemical shift index.

10.1021/bi702466a CCC: $40.75
Published on Web 06/18/2008

In this study, we have employed multidimensional NMR methods to monitor the aggregation of a truncated form of tau that efficiently and reproducibly aggregates into fibrils. We have identified a population of soluble oligomers of tau that appear in response to heparin-induced aggregation and which are amenable to NMR analysis. We identify two hexapeptide motifs in tau, VQIINK[280] and VQIVYK[311], that likely mediate intermolecular interaction between tau molecules to form oligomers associated with the aggregation process. This study provides insight into the early events in tau aggregation leading to pathological fibril formation.

MATERIALS AND METHODS

Tau[187] Expression and Purification. Residues 255−441 of the longest human tau isoform (two N-terminal repeats, four C-terminal repeats) were amplified by PCR, cloned into pET28 vector, and expressed in *Escherichia coli* strain BL21(DE3), resulting in "tau[187]" containing a hexahistidine tag (MGSSHHHHHHSSGLVPRGSH) fused to the N-terminus. *E. coli* was grown from a frozen glycerol stock in 10 mL of LB culture to OD_{600} 0.6−0.8. The LB culture (100 μL) was used to inoculate 200 mL of M9 minimal media and then grown overnight. The overnight culture (20 mL) was pelleted and resuspended into 500 mL of fresh M9MM supplemented with $^{15}NH_4Cl$ (1 g/L) and/or uniformly labeled ^{13}C glucose (2 g/L) (Cambridge Isotopes Laboratories Inc.). At OD_{600} 0.6−0.8, protein expression was induced with 1 mM isopropyl β-D-thiogalactoside for 3 h and then harvested by centrifugation for 15 min at 5000*g*. Pellets were stored at −80 °C until further use. All growth conditions were carried out at 37 °C. Mutants of tau[187] were generated using the QuickChange technique (Stragene).

Bacteria from the 1 L culture were washed and resuspended in 20 mL of lysis buffer (20 mM MOPS (pH 7.4), 10 mM imidizole, 0.1 mM EDTA, and 1 mM DTT) supplemented with PMSF (1 mM), leupeptin (0.5 μg/mL), aprotinin (2 μg/mL), and pepstatin A (0.7 μg/mL). After incubation with lysozyme (2 mg/mL, 15 min on ice), samples were sonicated (6 × 20 s at power setting 5 with 1 min cooling on ice between each sonication) in an ultrasonic cell disruptor (Branson Sonifier 250). The lysate was cleared by centrifugation (30 min at 15000 rpm, Sorvall SS-34), and the supernatant was batch loaded onto 2 mL of packed Ni-NTA agarose at 4 °C for 45 min. The resin was washed in a column with lysis buffer, followed by lysis buffer containing 250 mM NaCl, followed by lysis buffer. Protein was eluted with a 300 mM imidazole step. Fractions containing protein were pooled and applied to a column of SP-Sepharose (10 mL) equilibrated with 20 mM Tris (pH 8.2), 0.1 mM EDTA, 0.02% NaN_3, and 1 mM DTT, washed, and eluted with a NaCl gradient (0−500 mM NaCl/40 mL). Fractions were analyzed by SDS−PAGE; tau protein was pooled, concentrated to approximatey 1 mL using Amicon 4 mL centricon and applied to a CL6B Sepharose gel filtration column equilibrated with 20 mM sodium phosphate (pH 6.9), 100 mM NaCl, 0.1 mM EDTA, and 0.02% NaN_3. Protein was analyzed by SDS−PAGE, pooled, concentrated, and stored at −80 °C. Protein concentration was determined by absorbance at A_{274} assuming an extinction coefficient $\epsilon_{274} = 2.8\ cm^{-1}\ mM^{-1}$.

Derivatization of Tau with MTSL. Tau[187] (300−500 μM) was reduced for 2 h at room temperature with 10 mM DTT and then desalted on a 5 mL Sephadex gel filtration column (G-25 (80 mesh)) equilibrated with 20 mM sodium phosphate (pH 6.9), 100 mM NaCl, 0.1 mM EDTA, and 0.02% NaN_3. Tau[187] was immediately incubated with a 10-fold molar excess of (1-oxyl-2,2,5,5-tetramethylpyrrolidin-3-yl)methyl methanethiosulfonate (MTSL) spin label (Toronto Research Chemicals) for 16−18 h at 4 °C. Unreacted MTSL was removed using a 5 mL G-25-80 Sephadex gel filtration column equilibrated in 20 mM sodium phosphate (pH 6.9), 100 mM NaCl, 0.1 mM EDTA, and 0.02% NaN_3. To determine the extent of labeling, 20 μM tau[187] was reacted with 20 μM 2,2′-dithiodipyridine and quantified by absorbance at A_{343} (*23*). Spectrally inactive, diamagnetic MTSL-labeled protein was generated by reduction with 10 mM sodium ascorbate for 18 h in the dark at 4 °C. Ascorbate was removed by gel filtration. Samples were concentrated for NMR using a 0.5 mL Microcon centrifugal filter.

NMR Experiments and Data Analysis. All NMR data were collected at 25 °C on a Varian 600 MHz spectrometer equipped with a four-channel ($^1H/^{13}C/^{15}N/^2H$) room temperature or cryogenic probe and *Z*-axis pulsed field gradients. Uniformly ^{15}N- or $^{13}C/^{15}N$-labeled protein samples of tau[187] wild-type or mutants in NMR buffer (pH 6.9, 20 mM sodium phosphate, 0.1 mM EDTA, 100 mM NaCl, 0.01% NaN_3 in 92% H_2O/8% D_2O) were concentrated to 0.1−1.0 mM, depending on the experiment. The NMR buffer also contained 226 mM trimethylamine oxide (TMAO) (Sigma T0514), a natural osmolyte, unless otherwise indicated. For backbone and sequential assignments, we performed 2D $^1H-^{15}N$ HSQC and 3D HNCACB (*24, 25*), CBCA(CO)NH (*25, 26*), and HNCO (*26, 27*) experiments. The chemical shift reference is done with internal sodium 2,2-dimethyl-2-silapentane-5-sulfonate (DSS) at 0 ppm for its methyl proton signal, and the ^{13}C and ^{15}N chemical shifts are indirectly referenced. Data processing was done with the nmrPipe program package (*28*). All 3D data were processed with the maximum entropy method (MEM) in addition to the regular Fourier transform (FT) method. Data analysis and resonance assignments were made with a modified version of ANSIG (*29, 30*) running under the Linux operating system.

The backbone (*31*) ^{15}N NOE experiment was done with a 3 s ^1H saturation period during a total of 8 s recycle delay and compared with the one without ^1H saturation. Paramagnetic relaxation enhancements (PRE) were measured from the peak intensity ratios between two $^1H-^{15}N$ HSQC spectra acquired at the same time point after mixing ^{15}N-tau[187] with oxidized versus reduced MTSL-labeled ^{14}N-tau[187]. In all experiments, ^{15}N-tau[187] corresponding mutant was not labeled with MTSL. A $^1H-^{15}N$ HSQC spectrum was collected after mixing ^{15}N-tau[187] and MTSL-^{14}N-tau[187] but before heparin addition. After heparin addition, a series of $^1H-^{15}N$ HSQC spectra were collected continuously up to times ranging from 3 to 16 h. Each spectrum was acquired over 32 min and was done with eight scans, 100 ^{15}N increments, a recycle delay of 1 s, and spectral width of 1124 Hz for ^{15}N and 9000 Hz for ^1H. There was a 4 min dead time between addition of heparin and data collection. Aggregation experiments contained 150 μM ^{15}N tau[187] unlabeled mutant and 300 μM ^{14}N tau[187] MTSL derivative. Final volume was 450 μL. The

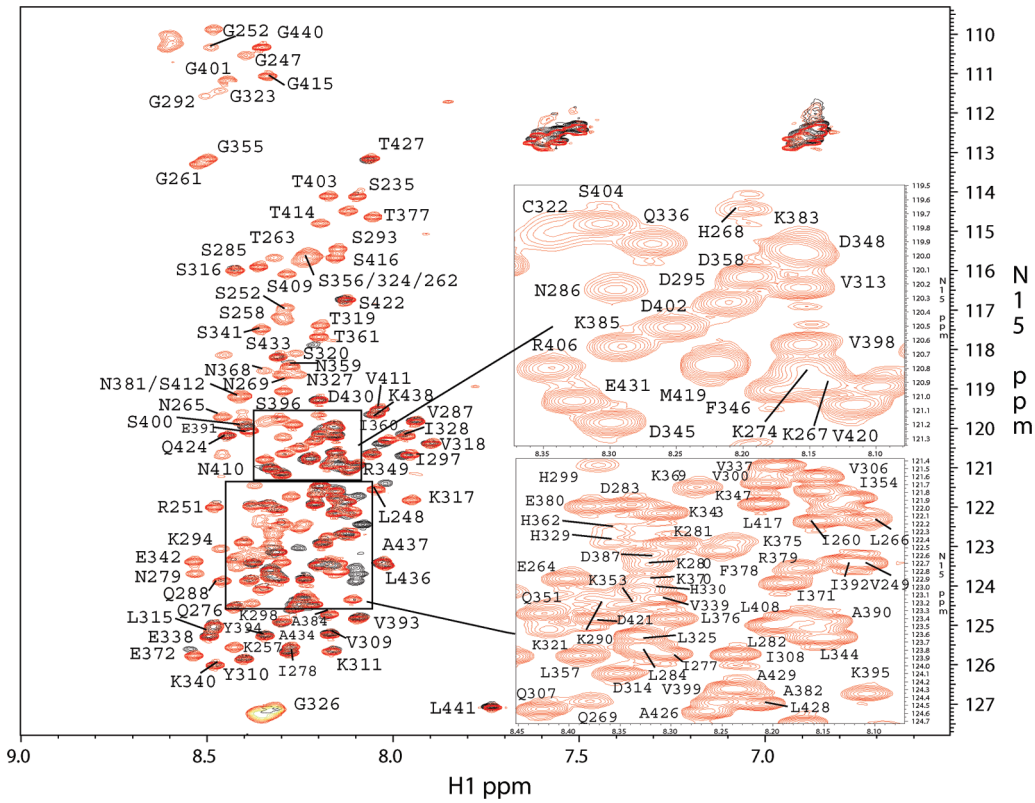

FIGURE 1: $^{1}H-^{15}N$ HSQC spectra of tau^{187}. The spectra of Tau^{287} with (red) and without (black) 226 mM TMAO are superimposed. The spectra were collected at 25 °C with 0.5 mM protein in a buffer containing 20 mM sodium phosphate, pH 6.9, 100 mM NaCl, 0.1 mM EDTA, 0.02% NaN_3, and 8% D_2O.

molar ratio of heparin (Sigma H3400, MW ~3 kDa) to tau^{187} was kept constant at 1:5 in all experiments.

Mass Spectroscopy. ^{15}N-tau^{187} C291S was labeled with MTSL at residue 322, as described above for ^{14}N-tau^{187} mutants. The corresponding ^{14}N-tau^{187} C291S mutant was left unlabeled, and the protein samples were mixed in a 2:1 ratio (100 μL, 450 μM) and applied to a 1 mL G25-80 spin column with or without incubation with 3 kDa heparin for 2 h and then eluted into nanopure water. Mass spectrometry was performed using a Micromass QTOF2 quadrupole/time-of-flight tandem mass spectrometer in positive ion mode. MassLynx (Micromass Inc.) software provided with the mass spectrometer permitted mass spectra to be displayed for any observed peak of ion detection events, allowed background subtraction, as well as extraction of a defined input *m/z* from the data set.

Transmission Electron Microscopy. After aggregation, 10 μL of sample was applied to a 300 mesh Formvar/carbon-coated copper grid for 90 s, excess liquid in the sample was wicked using filter paper and stained with 10 μL of 1.5% uranyl acetate for 30 s, wicked again, and washed with 10 μL of H_2O for 90 s, wicked again, and air-dried. Samples were analyzed using a JEOL JEM-1230 transmission electron microscope.

RESULTS

Backbone Resonance Assignments for Tau^{187}. We engineered a truncated fragment of the tau molecule comprising the complete microtubule-binding repeat region followed by the C-terminal tail of the longest tau isoform. This fragment, tau^{187}, undergoes rapid aggregation upon addition of heparin and generates PHF-like fibers as observed by electron microscopy (*32*). In the experiments that follow, we employed tau^{187} to study the aggregation process by multidimensional NMR.

Analysis of tau^{187} by two-dimensional NMR (Figure 1) is consistent with the accepted view that full-length tau is an unstructured molecule under native conditions when free in solution (*9, 15–17, 19*). In particular, the 2D $^{1}H-^{15}N$ HSQC NMR spectrum revealed proton dispersion spanning approximately 0.5 ppm (Figure 1). Resonance peaks were broad and overlapping, and under these conditions we were unable to assign most of these peaks.

We previously demonstrated the effects of the natural osmolyte, TMAO, which dramatically enhances the kinetics of tau aggregation (*32*). As an extension of this work, we herein asked how TMAO may affect the structure of tau analyzed by NMR. In TMAO, tau^{187} displayed sharper and more highly resolvable resonance peaks up to concentrations of 1.6 M TMAO. It is possible that the increased resolution seen with TMAO could reflect slower amide exchange with solvent. However, one would expect a range of hydrogen exchange rates reflecting the type of amino acid residue and its near neighbors (*33*). We do not observe the expected differential broadening due to amide exchange. Rather, we attribute these effects of TMAO to a greater constraint on the conformational space available for sampling by tau^{187} that diminishes contributions from slower processes. In 226 mM TMAO, we were able to assign 155 of the 187 residues in tau^{187} (Figure 1). Residues that could not be assigned were largely confined to the C-terminal ends of the MT-binding repeat domains which have the sequence XXPGGG (residues 268−274, 300−304, 329−334, 363−366). The assignment

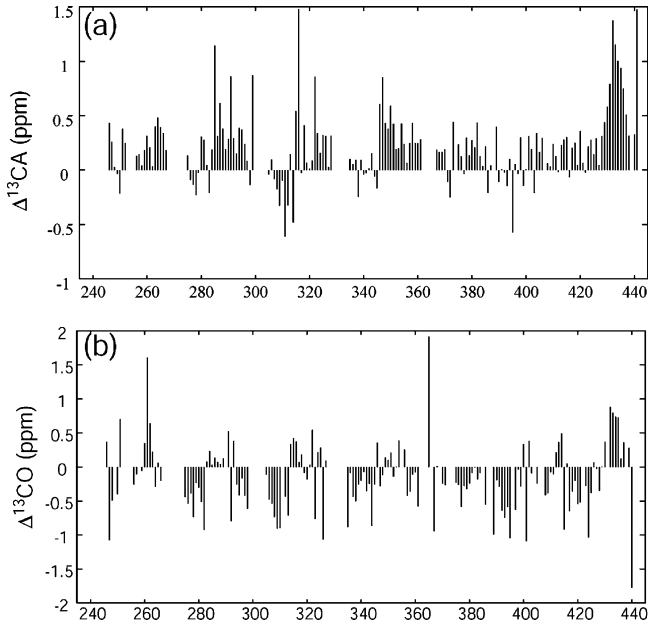

FIGURE 2: Chemical shift deviations of tau[187] from values for random coil peptides. Data were collected in NMR buffer containing 20 mM sodium phosphate, 0.1 mM EDTA, 100 mM NaCl, and 0.01% NaN_3 in 92% H_2O/8% D_2O, pH 6.9. Positive deviations represent helical propensity; negative deviations represent propensity for extended structure. The chemical shift values of CA and CO nuclei for random coil peptides were taken from Wishart et al. [(1995) *J. Biomol. NMR 5*, 67−81], and corrections were made to the shift values of residues followed by a proline accordingly.

of two histidine residues of tau[187] (His388, His407) also could not be made.

Analysis of the chemical shift index (CSI) (*34, 35*) of assigned residues revealed moderate α-helical character throughout the molecule (Figure 2). Strong propensity for secondary structure was apparent only in the region of residues 308−312 whose CSI values suggest *β*-sheet character. The CSI profile did not change in the absence of TMAO (not shown), suggesting minimal overall secondary structure induced by this agent. These results are highly similar to those of Eliezer et al. (*36*) and Sibelle et al. (*37*), who also demonstrate mostly α-helical content in K19 with exception of the region corresponding mainly to the PHF6 motif (VQIVYK[311]), which is strongly *β*-sheet. On the other hand, Mukrasch et al. (*38*) observed significantly more *β*-sheet propensity throughout the K18 and K19 molecules based on Cα chemical shift values. Several standard CO chemical shift tables for random coil peptides have been proposed. These differ significantly, likely due to higher sensitivity of CO atoms to environmental effects than Cα atoms. Thus, secondary structure prediction using chemical shifts of CO nuclei is less reliable than using those of Cα nuclei, particularly for the prediction of *β*-strand structure (*34, 39, 40*). Nevertheless, the consensus among several NMR studies is that the core region containing the PHF6 motif likely has residual *β*-strand structure. Other regions of tau likely possess helical character, but further research is needed to confirm this point.

We also obtained [^{1}H]^{15}N NOE data for tau[187] (not shown). [^{1}H]^{15}N NOEs measure the effect of the dipole−dipole interaction between two adjacent spins and are sensitive to fast, ps to ns motions. Values range from negative, when the overall correlation time is in the ps range corresponding to high flexibility, to positive, when the correlation time is a few ns or longer often seen in rigid parts of the molecule. In the absence of TMAO, positive NOE values were not observed, indicating the lack of any segmental rigidity of significant persistence length. In TMAO (226 mM), however, several positive [^{1}H]^{15}N NOEs appeared. These peaks corresponded to residues in interrepeat regions two and three and within the C-terminal tail region, suggesting some rigidity that is induced in these regions by TMAO. In the absence of any other obvious structural differences, the change in protein dynamics may be the cause of the dramatically enhanced propensity of tau to aggregate into fibers in TMAO (*32*).

Site-Specific Spin Labeling. The overall lack of defined structure in tau[187] led us to carry out site-specific paramagnetic spin labeling with the goal of mapping long-range intermolecular interactions by paramagnetic resonance enhancement (PRE) of resonance peak broadening. Tau contains two endogenous cysteine residues. We engineered four tau mutants to contain single cysteine residues at positions 258 (S258C/C291S/C322S), 291 (C322S), 322 (C291S), and 356 (S356C/C291S/C322S) for subsequent reaction with the nitroxide spin-label, MTSL. The corresponding MTSL-labeled proteins are referred to as SL258, SL291, SL322, and SL356, respectively. Each of these proteins was incorporated with either ^{14}N or ^{15}N nitrogen. The ^{14}N mutants were then reacted with MTSL on the single cysteine residue present. The corresponding MTSL-^{14}N-tau[187] and ^{15}N-tau[187] mutants were then mixed at 2:1 ratio, and resonance peaks observed by 2D H^1-N^{15} HSQC were analyzed before and immediately after induction of aggregation by heparin.

Each site-specific spin-labeled mutant displayed a single set of ^{1}H−^{15}N HSQC resonances with specific resonances that were significantly broadened by interaction with the MTSL label on ^{14}N-tau[187] (Figure 3). The enhanced broadening of resonance peaks (Figure 3) is necessarily due to intermolecular interaction between ^{15}N- and ^{14}N-tau[187] molecules, because the MTSL label is present only on ^{14}N-tau[187]. The MTSL label did not undergo intermolecular exchange from ^{14}N to ^{15}N-tau in either the presence or absence of heparin, as determined by mass spectrometry analysis (Figure 4). Thus the NMR signal observed must correspond to a soluble oligomer of tau consisting of at least two tau molecules that forms only upon heparin induction. The exact number of tau molecules in the oligomer is not known. The observation that line broadening occurs specifically in response to heparin addition suggests that the oligomer may in some way be associated with fiber formation.

Figure 3 shows that in all MTSL-labeled mutants two peaks of resonance broadening were observed. Remarkably, the same two regions in tau were broadened in all spin-labeled mutants. This broadening cannot be attributed to direct interaction between tau and heparin itself, because broadening was not observed when the MTSL spin label was reduced to diamagnetic MTSL by ascorbic acid. Broadening also cannot be due to nonspecific effects of the MTSL label itself, because the spectra after inactivation of MTSL was the same as that when unlabeled ^{14}N-tau was employed, in either the presence or absence of heparin (not shown).

The fact that the broadened regions in tau were the same regardless of the position of the MTSL label caused concern that the MTSL label may display nonspecific interaction with

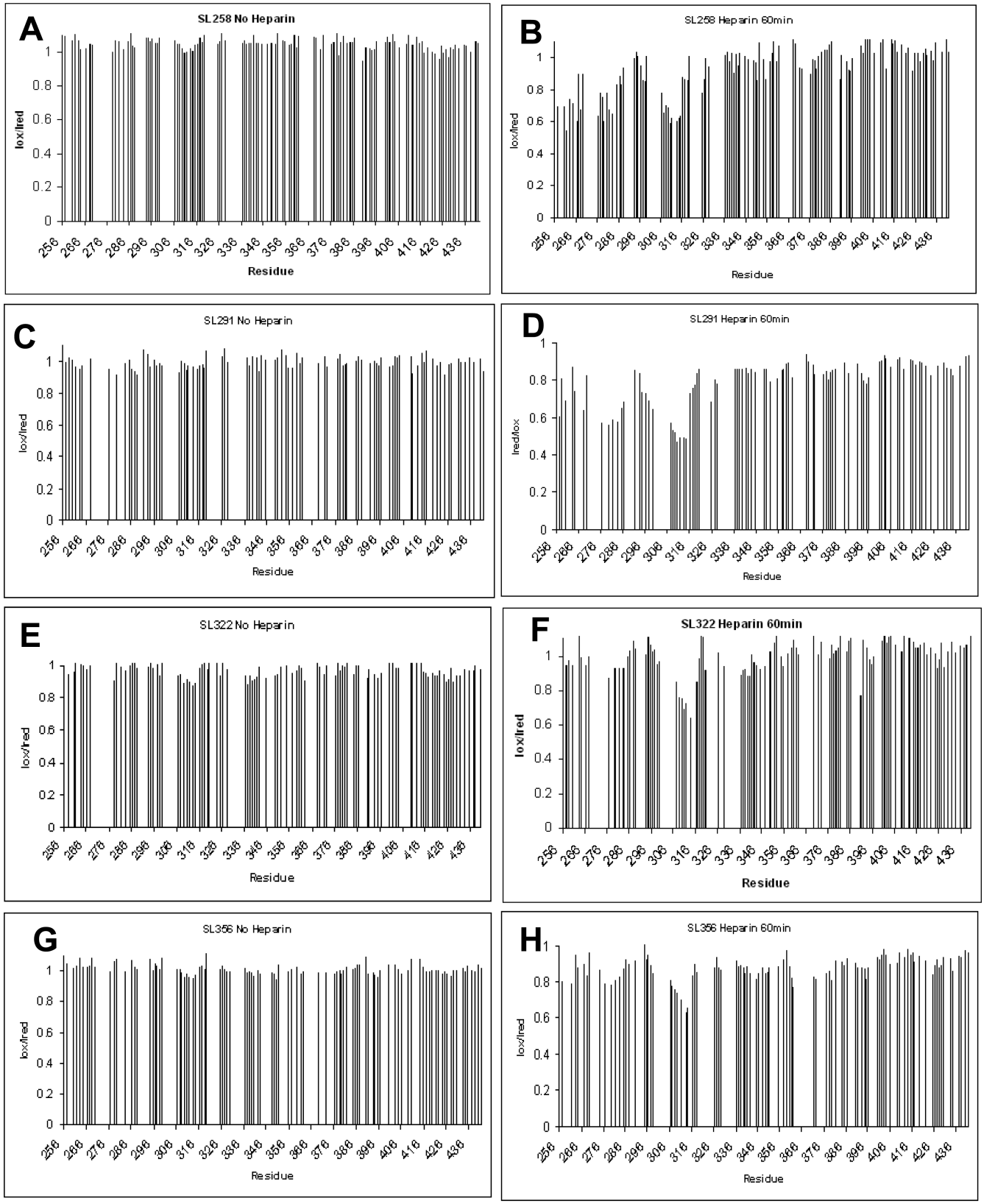

FIGURE 3: Paramagnetic relaxation enhancements of ^{15}N-tau^{187} from MTSL spin-labeled ^{14}N-tau^{187}. ^{15}N-tau^{187} was mixed with ^{14}N-tau^{187} labeled with either paramagnetic or diamagnetic MTSL. PRE values represent peak intensity ratios of paramagnetic vs diamagnetic MTSL-^{14}N-tau^{187} as described in Materials and Methods. (A, B) SL258; (C, D) SL291; (E, F) SL322; (G, H) SL356. MTSL at any of the indicated four positions in tau results in the same two peaks of broadening upon initiation of aggregation, corresponding to the regions VQIINK^{280} and VQIVYK^{311}.

these regions. Therefore, even though broadening was clearly heparin-dependent, we tested if the corresponding resonance peaks would be broadened by free MTSL. An MTSL−mercaptoethanol derivative free in solution was tested for this purpose and was found not to result in broadening when present at equivalent concentrations of MTSL-^{14}N-tau (Figure

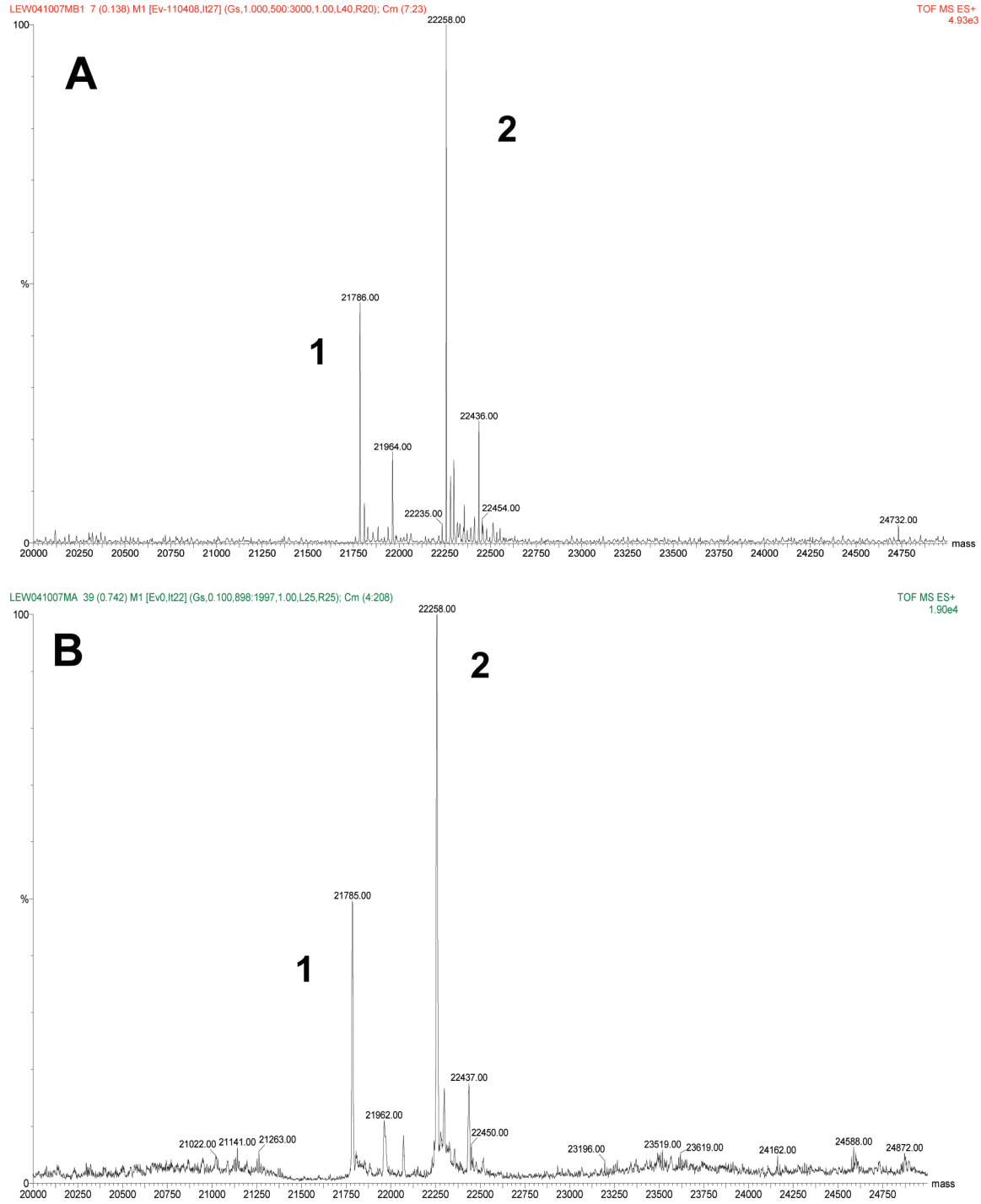

FIGURE 4: Mass spectrometry of SL-tau[187]. MTSL was reacted with ^{15}N-tau[187] at residue 322. The spin-labeled ^{15}N-tau[187] (peak 2) and the corresponding unlabeled ^{14}N-tau[187] mutant (peak 1) were mixed in 2:1 ratio and analyzed by ESI mass spectrometry in positive ion mode (A) before heparin addition and (B) 2 h after addition of 90 μM 3 kDa heparin. Masses of peaks 1 and 2 remain unchanged after heparin addition, demonstrating that the spin label does not exchange with free thiol in ^{14}N-tau[187].

5A,B). Furthermore, we engineered a cysteine residue at a remote site in the C-terminus of tau (aa 413) and found that MTSL at this position produced some minimal broadening around residues 416 and 430 (Figure 5C,D) but did not produce the specific broadening seen in Figure 3. These data suggest that this broadening (Figure 3) is a specific paramagnetic relaxation enhancement effect of MTSL at positions 258, 291, 322, and 356.

Enhanced line broadening is a direct function of the fraction of oligomer, f, the correlation time of the specific residue, τ, and an inverse function of the distance, r, between MTSL and the specific residue raised to the sixth power (PRE ∞ $f\tau/r^6$). Since identical regions in tau are specifically broadened in response to MTSL located at various positions, we propose that line broadening must be dominated by a combination of the proximity of the nitroxide to a particular nuclear spin as well as the flexibility of the region including that nuclear spin. We imagine that the PHF6 hexapeptide regions make transient contact that both stiffens the region and brings the nitroxide label to the vicinity. To test if these regions are flexible in the monomer, we labeled ^{15}N-tau[187] with MTSL directly and under these conditions did not

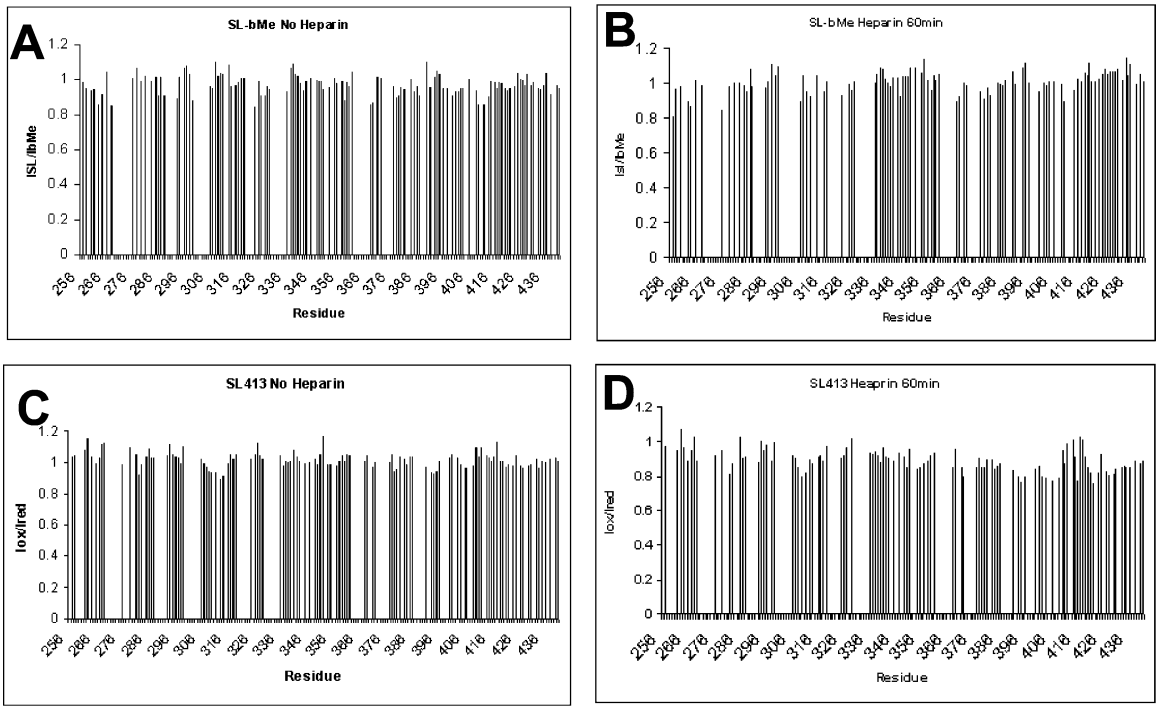

FIGURE 5: PRE effect of free MTSL and MTSL linked to residue 413. (A, B) PRE effects from free MTSL derivatized with mercaptoethanol were tested on ^{15}N-tau. The ratio of peak intensities of ^{15}N-tau alone vs ^{15}N-tau in the presence of 300 μM MTSL−mercaptoethanol is shown. (C, D) PRE effects of MTSL at position 413 in the C-terminus of tau.

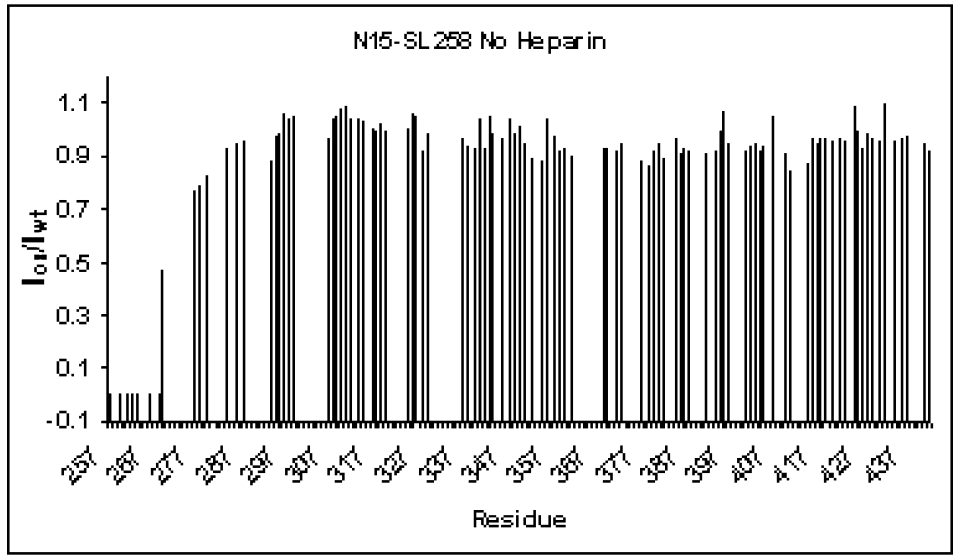

FIGURE 6: Paramagnetic relaxation enhancements of ^{15}N-tau^{187} labeled with MTSL. ^{15}N-tau^{187} containing a single cysteine residue at position 258 was generated and labeled with MTSL as described in Materials and Methods. Line broadening was observed by HSQC analysis. In the absence of heparin, MTSL caused broadening of adjacent residues but not residues within the VQIINK^{280} or VQIVYK^{311} regions, suggesting that in the absence of heparin these regions are flexible. PRE effects are given as the ratio of MTSL-labeled to unlabeled ^{15}N-tau^{187}. Experiments were done at 100 μM tau protein in NMR buffer (see Materials and Methods).

observe enhanced broadening at these regions (Figure 6). Thus broadening is seen only in the oligomer as opposed to the monomer, suggesting that these regions become stiff specifically in response to aggregation, most likely due to intermolecular contact between tau^{187} molecules at these regions.

The two regions in tau^{187} displaying broadened resonances (Figure 3) correspond to the motifs VQIINK^{280} and VQIVYK^{311}. It has previously been shown that a short fragment of tau (N265−E335) containing VQIVYK^{311} can bind to small immobilized peptides which themselves contain either VQIINK^{280} or VQIVYK^{311} and that the sequence VQIVYK^{311} is important for aggregation (*15*), being able to aggregate into straight fibers on its own (*41*). Our data are consistent with both motifs making intermolecular contact with one or the other cognate sequence during the aggregation process, resulting in stiffening of each respective motif and an increase in correlation time with consequent line broadening.

While there is evidence to suggest that tau molecules in mature fibers are homogenously stacked in parallel and in register, the NMR data on the oligomer cannot easily be explained by a single species. Parallel, in-register stacking (Figure 7, structure A) can explain the line broadening in

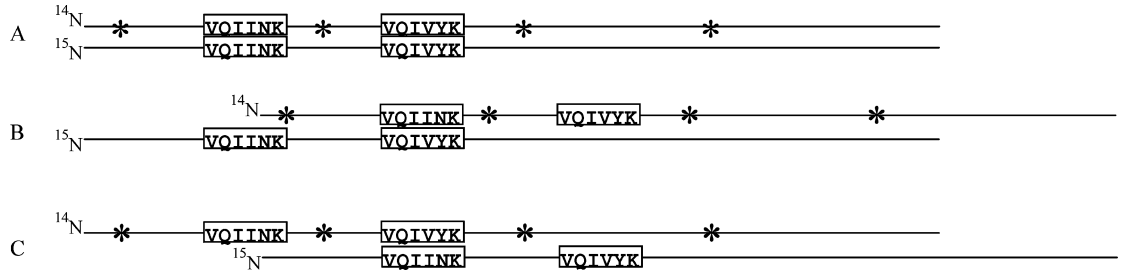

FIGURE 7: Possible tau complexes generated during aggregation. The region in tau between residues 258−~400 is depicted. Asterisks indicate the positions of single MTSL derivatizations in relation to the regions observed to be broadened: VQIINK[280] and VQIVYK[311]. Broadening seen with MTSL at SL258, SL291, SL322, and SL356 can be explained by a mixture of structures A, B, and C. Other structures including antiparallel complexes are also possible.

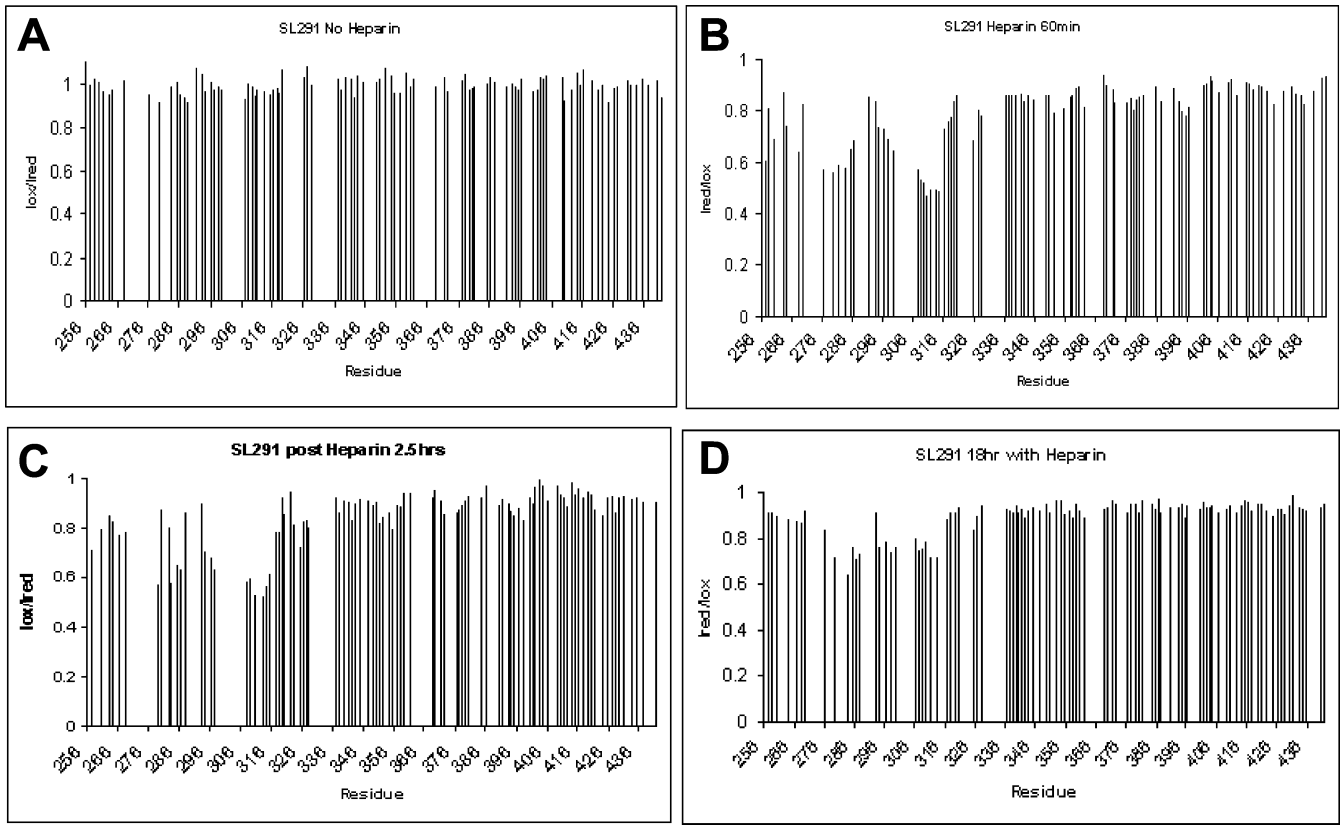

FIGURE 8: Time course of peak broadening. PRE effects in SL291 were followed over time. Peak broadening was maximal at 1 and 2.5 h and diminished over time, suggesting that formation of the soluble oligomer is transient. PREs are given as the ratio of broadening due to paramagnetic vs diamagnetic MTSL as described in Materials and Methods and in the legend to Figure 3. SL322 displayed a similar time course (not shown).

SL291, SL322, and SL356 but not in SL258 for which both broadened peaks are of roughly equal intensity. The simplest explanation involves multiple species that include structure A as well as a form with parallel shifted register, B (Figure 7). If B forms, C must also form in corresponding amounts, since B and C are identical structures if tau is unlabeled. The coexistence of structures A, B, and C explain the pattern of broadening that we observe. However, we cannot rule out the existence of other complexes involving combination of parallel and/or antiparallel arrangements. In all cases, the amplitude of peak broadening was significantly less than that expected if all tau molecules were present as an oligomer, suggesting that the population of monomer over total oligomer is favored. In summary, our data suggest that a small heterogeneous population of oligomeric complexes forms after initiation of aggregation as part of a search for the specific species that is active in promoting fiber formation.

As further evidence that the oligomer may be an intermediate species related to the fiber forming process, we examined the time course of line broadening. Broadening occurred transiently over time peaking between 1−2.5 h after the initiation of aggregation (Figure 8). At 18 h, broadening was significantly reduced. The transient nature of the broadening has previously been observed by Mukrasch et al. (*38*) and is consistent with an intermediate that initially accumulates and then decays as substrate is depleted. In this case, we speculate that disappearance of the oligomer correlates with its sequestration into fibers as the heparin runs out. This is consistent with studies showing that heparin is limiting under the conditions of aggregation used for NMR (Peterson et al., unpublished). Finally, to ensure that heparin-stimulated aggregation results in fiber formation, we visualized tau by EM after heparin addition. Copious fibers reminiscent of bona fide PHFs were apparent in the SL258,

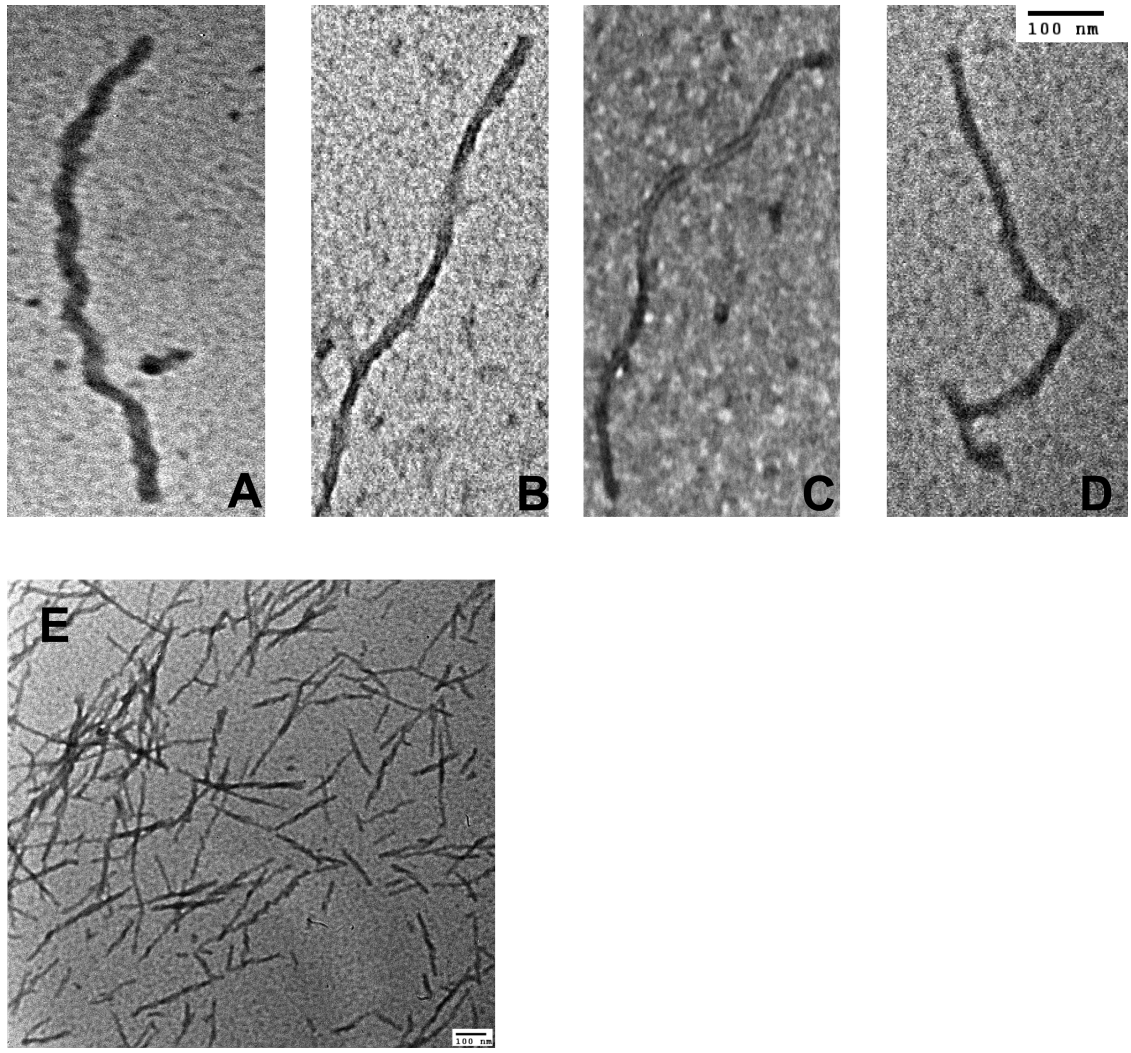

FIGURE 9: Transmission electron microscopy of fibers formed from MTSL-tau^{187} mutants. MTSL-tau^{187} was analyzed for fiber formation by transmission EM after 16 h of heparin-induced aggregation. (A) SL258; (B) SL291; (C) SL322; (D) SL356 (all at 120000× magnification); (E) SL322 (80000× magnification).

SL291, SL322 and SL356 spin-label mutants 16 h after heparin addition (Figure 9).

DISCUSSION

The aggregation of tau into paired helical filaments is believed to be critical for the progression of Alzheimer's disease. Yet the mechanism by which tau, a soluble and intrinsically unstructured molecule, undergoes self-assembly to form insoluble filaments with regular secondary structure is not known. Soluble oligomers have been identified as intermediates in protein filament formation (*42*), including tau fiber formation (*43*). Using multidimensional NMR methods, we have identified a population of soluble oligomers of tau that transiently accumulate upon initiation of aggregation by heparin. Although we cannot say whether one or more of these species are on the pathway to fiber formation, the formation of these oligomers occurs specifically during the aggregation process and correlates with intermolecular interaction between the PHF6 and PHF6* hexapeptide motifs of two tau molecules, these motifs of which have been shown to be essential and sufficient for aggregation (*15, 41*)

Tau has resisted all attempts of high-resolution structural characterization by X-ray crystallographic or NMR methods. A principal reason for this is that tau free in solution is an intrinsically unstructured molecule under native conditions, while fibrous tau, which is known to contain regular secondary structure, is insoluble. Previous attempts to crystallize the soluble protein resulted in fiber formation (*12*), and the large size (441 amino acids) of full-length tau has precluded high-resolution structural characterization by NMR. Here, we have engineered a truncation fragment of tau, tau^{187} (aa 255−441), which comprises all four microtubule binding repeat regions along with the C-terminal tail domain of the molecule. This fragment retains full aggregation activity and upon aggregation forms fibers identical to those generated from full-length tau in vitro, or fibers isolated from Alzheimer's brain tissue (*32*).

Trimethylamine *N*-oxide (TMAO) is a natural osmolyte found in marine animals that serves to counteract the protein denaturing effects of high urea concentrations encountered in the normal life of these organisms (*44, 45*). TMAO acts by stabilizing the native fold of proteins and, in the absence of denaturant, can promote the folding of proteins into their native structures in vitro (*46–49*). In our hands, we found that moderate concentrations of TMAO were critical to allow assignment of 30 resonance peaks that were otherwise unobservable, along with a large number of resonance peaks

that were overlapping and unresolvable in the absence of TMAO. In TMAO we were able to assign 85% of the $^{1}H-^{15}N$ HSQC resonance peaks in tau[187].

We could not carry out experiments using spin-labeled tau in the absence of TMAO due to the inability to assign the majority of resonance peaks. Thus, one could argue that the PRE effects that we observe may be a TMAO-specific phenomenon. However, evidence suggests that our results herein are relevant to tau aggregation in general. First, it has previously been demonstrated that TMAO promotes the ability of tau to assemble tubulin into microtubules (*50*) and dramatically enhances the aggregation of tau[187] to form fibers (*32*), suggesting that TMAO acts to promote processes that are physiologically relevant, consistent with its known chaperone activity. Second, fibers formed in the presence of TMAO are structurally identical to fibers formed without TMAO, as observed by electron microscopy (*32, 50*). Third, our results implicating the PHF6 and PHF6* hexapeptide motifs as key tau interaction domains during aggregation are consistent with previous studies (*15, 41*). Finally, the secondary structure propensity of tau[187] in our hands is the same as that reported in previous studies carried out without TMAO (*36, 37*).

NMR assignments for tau and a number of tau fragments in the absence of TMAO have previously been reported. Lippens et al. (*51*) first reported assignments of full-length tau which corresponded to TP and SP motifs in the primary sequence, followed by Smet et al. (*52*), who assigned 30% of residues in full-length tau unambiguously and another 10% with certainty between two possible amino acid choices. These studies confirm the lack of abundant secondary structure in tau. Eliezer et al. (*36*) reported the assignment of 90 out of 98 amino acids in a fragment of tau, K19, corresponding to the microtubule binding repeat region of three-repeat tau, while Mukrasch et al. (*38*) made nearly complete assignments of K19 and the corresponding fragment from four-repeat tau, K18 (120 amino acids), with the exception of several Gly residues. The largest fragment of tau recently resolved by NMR is a 198 amino acid fragment, corresponding to the four-repeat microtubule binding domain plus neighboring flanking sequences, for which approximately 95% of the residues have been assigned (*53*). This fragment is similar to tau[187] in that it spans the four-repeat region but differs by including the second proline-rich domain and lacks the complete C-terminal tail. The published assignments of these fragments agree with the assignments we report in this study on tau[187].

The enhanced relaxation of $^{1}H-^{15}N$ HSQC resonance peaks in the presence of MTSL-^{14}N-tau[187] (Figure 3) suggests that a soluble oligomer of two or more tau molecules must form in response to heparin. Resonance broadening via an intramolecular mechanism is not possible because ^{15}N-tau[187] does not contain MTSL in these experiments. Second, the MTSL label does not exchange from ^{14}N- to ^{15}N-tau over the time period in which our experiments were conducted (Figure 4). Finally, the peaks of broadened residues in each ^{15}N-tau mutant do not correspond to the location of the MTSL label in the primary sequence of ^{14}N-tau. Thus resonance broadening must reflect intermolecular interaction between tau molecules.

The large size of the fibers makes it unlikely that fibers contribute significantly to the NMR signal, supported by the fact that resonance peaks are sharp and that the association kinetics of oligomer binding is most likely too slow for detection by NMR. For example, an upper limit estimate of 1 million fibers in 1 μL would correspond to a concentration of 10^{-12} M fiber ends. Even if the overall bimolecular encounter between oligomer and fiber were diffusion controlled (10^{8} M^{-1} s^{-1}), the apparent first-order association rate constant (10^{-4} s^{-1}) would be expected to be too slow to produce the observed fast chemical exchange of monomers into the fiber.

Scheme 1

Scheme 2

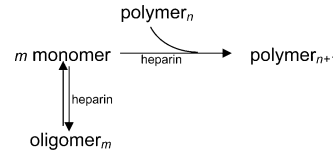

Previous studies have shown that the hexapeptide motifs, VQIINK[280] and VQIVYK[311], within the microtubule-binding region of tau can stably interact with each other as well as with themselves when tested independently as peptides (*15*) and that VQIVYK[311] can aggregate into fibers on its own (*41*). Our NMR data are consistent with these motifs being sites of intermolecular interaction in the oligomer and, hence, provide evidence that interaction at these sites may be key during the process of aggregation. We propose that upon interaction these regions stiffen, resulting in a decrease in their correlation time. This is based on the fact that we see broadening exclusively at these regions in each of the four MTSL-labeled mutants as opposed to other regions in the molecule that are presumably closer to the MTSL label but are necessarily more flexible.

Studies suggest that in mature fibers tau molecules are aligned homogensously in parallel and in register (*21*). By comparison, our studies show that a population of soluble oligomers of tau induced by heparin likely does not correspond to a single species. Rather, multiple oligomeric species likely exist including species that are not in register. The minimum species to explain the enhanced relaxation patterns is shown in Figure 7. Given this, two scenarios (Schemes 1 and 2) for fiber formation are possible in which the oligomer$_m$ designates a heterogeneous oligomeric population.

In both schemes, tau monomers may transiently interact to explore the energy landscape of possible complexes. The idea that protein−protein association involves transient complexes that eventually settle into the most thermodynamically favored state(s) has been seen in other systems (*54*). Interconversion between monomer and oligomer complex is assumed to be rapid, suggested by the single, sharp resonance peaks corresponding to individual residues observed by HSQC analysis. The population of monomer is favored over oligomer, suggested by the degree of peak broadening, which is less than maximal. Our data do not discern between Schemes 1 and 2. However, studies show that tau dimers as opposed to monomers favor aggregation kinetics (*9*), suggesting that Scheme 1 is more likely if this is true.

Recent NMR studies have identified potential residues in tau that interact with both polyanion inducers of tau aggregation and microtubules. Mukrasch et al. identified heparin binding to the PHF6 and PHF6* motifs, while Sibille et al. (*37*) reported high-affinity binding of heparin to residues within PHF6. It is unclear from either of these studies, however, whether or not the observed chemical shifts of these residues can alternatively be attributed to tau−tau interactions in response to heparin-induced aggregation. While Sibille et al. (*37*) used a low MW (4.2 kDa) heparin species which could bind but not cause aggregation of full-length tau, we observed robust aggregation of tau^{187} initiated with a 3 kDa heparin species. Like Mukrasch et al. (*38*) and Sibille et al. (*37*), we propose that PHF6 and PHF6* are targets of molecular interaction in response to heparin addition. But, in contrast, we show unequivocally through the use of paramagnetic versus diamagnetic MTSL spin-label probes attached to ^{14}N-tau^{187} that line broadening at these hexapeptide motifs in ^{15}N-tau^{187} cannot be caused by heparin directly. We attribute the observed PRE effects to intermolecular tau−tau interactions triggered by heparin addition. Since we do not know where heparin binds from this study, we do not yet conclude that our results are mutually conflicting with the results of Mukrasch et al. (*38*) and Sibille et al. (*37*).

Our studies demonstrate that soluble oligomers of tau observable by NMR are generated during the process of aggregation and fiber formation. We propose that the regions VQIINK^{280} and VQIVYK^{311} are the major sites of intermolecular interaction in the oligomer population during the early process of aggregation and that these interactions that generate the oligomer are triggered in response to heparin addition possibly serving as seeds of nucleation. In the future, it will be of interest to correlate defects in aggregation by site-directed mutagenesis with possible changes in the dynamics of the soluble oligomeric species of tau observable by NMR methods. Ultimately, characterization of the kinetic pathway of tau aggregation may guide the design of small molecule therapeutic inhibitors of neurofibrillary tangle formation.

REFERENCES

1. Selkoe, D. J. (1986) Altered structural proteins in plaques and tangles: what do they tell us about the biology of Alzheimer's disease? *Neurobiol. Aging 7*, 425–432.
2. DeMager, P. P., Penke, B., Walter, R., Harkany, T., and Hartignny, W. (2002) Pathological peptide folding in Alzheimer's disease and other conformational disorders. *Curr. Med. Chem. 9*, 1763–1780.
3. LaFerla, F. M., and Oddo, S. (2005) Alzheimer's disease: Abeta, tau and synaptic dysfunction. *Trends Mol. Med. 11*, 170–176.
4. Mandelkow, E., and Mandelkow, E. M. (1995) Microtubules and microtubule-associated proteins. *Curr. Opin. Cell Biol. 7*, 72–81.
5. Delacourte, A., and Buee, L. (1997) Normal and pathological Tau proteins as factors for microtubule assembly. *Int. Rev. Cytol. 171*, 167–224.
6. Andreadis, A. (2005) Tau gene alternative splicing: expression patterns, regulation and modulation of function in normal brain and neurodegenerative diseases. *Biochim. Biophys. Acta 1739*, 91–103.
7. Crowther, T., Goedert, M., and Wischik, C. M. (1989) The repeat region of microtubule-associated protein tau forms part of the core of the paired helical filament of Alzheimer's disease. *Ann. Med. 21*, 127–132.
8. Lee, G., Neve, R. L., and Kosik, K. S. (1989) The microtubule binding domain of tau protein. *Neuron 2*, 1615–1624.
9. Barghorn, S., and Mandelkow, E. (2002) Toward a unified scheme for the aggregation of tau into Alzheimer paired helical filaments. *Biochemistry 41*, 14885–14896.
10. Friedhoff, P., Schneider, A., Mandelkow, E. M., and Mandelkow, E. (1998) Rapid assembly of Alzheimer-like paired helical filaments from microtubule-associated protein tau monitored by fluorescence in solution. *Biochemistry 37*, 10223–10230.
11. Goedert, M., Jakes, R., Spillantini, M. G., Hasegawa, M., Smith, M. J., and Crowther, R. A. (1996) Assembly of microtubule-associated protein tau into Alzheimer-like filaments induced by sulphated glycosaminoglycans. *Nature 383*, 550–553.
12. Giannetti, A. M., Lindwall, G., Chau, M. F., Radeke, M. J., Feinstein, S. C., and Kohlstaedt, L. A. (2000) Fibers of tau fragments, but not full length tau, exhibit a cross beta-structure: implications for the formation of paired helical filaments. *Protein Sci. 9*, 2427–2435.
13. Berriman, J., Serpell, L. C., Oberg, K. A., Fink, A. L., Goedert, M., and Crowther, R. A. (2003) Tau filaments from human brain and from in vitro assembly of recombinant protein show cross-beta structure. *Proc. Natl. Acad. Sci. U.S.A. 100*, 9034–9038.
14. Barghorn, S., Davies, P., and Mandelkow, E. (2004) Tau paired helical filaments from Alzheimer's disease brain and assembled in vitro are based on beta-structure in the core domain. *Biochemistry 43*, 1694–1703.
15. von Bergen, M., Friedhoff, P., Biernat, J., Heberle, J., Mandelkow, E. M., and Mandelkow, E. (2000) Assembly of tau protein into Alzheimer paired helical filaments depends on a local sequence motif ((306)VQIVYK(311)) forming beta structure. *Proc. Natl. Acad. Sci. U.S.A. 97*, 5129–5134.
16. Schweers, O., Schonbrunn-Hanebeck, E., Marx, A., and Mandelkow, E. (1994) Structural studies of tau protein and Alzheimer paired helical filaments show no evidence for beta-structure. *J. Biol. Chem. 269*, 24290–24297.
17. Cleveland, D. W., Hwo, S. Y., and Kirschner, M. W. (1977) Physical and chemical properties of purified tau factor and the role of tau in microtubule assembly. *J. Mol. Biol. 116*, 227–247.
18. Woody, R. W., Clark, D. C., Roberts, G. C., Martin, S. R., and Bayley, P. M. (1983) Molecular flexibility in microtubule proteins: proton nuclear magnetic resonance characterization. *Biochemistry 22*, 2186–2192.
19. Wille, H., Drewes, G., Biernat, J., Mandelkow, E. M., and Mandelkow, E. (1992) Alzheimer-like paired helical filaments and antiparallel dimers formed from microtubule-associated protein tau in vitro. *J. Cell Biol. 118*, 573–584.
20. Kirschner, D. A., Abraham, C., and Selkoe, D. J. (1986) X-ray diffraction from intraneuronal paired helical filaments and extraneuronal amyloid fibers in Alzheimer disease indicates cross-beta conformation. *Proc. Natl. Acad. Sci. U.S.A. 83*, 503–507.
21. Margittai, M., and Langen, R. (2004) Template-assisted filament growth by parallel stacking of tau. *Proc. Natl. Acad. Sci. U.S.A. 101*, 10278–10283.
22. Santacruz, K., Lewis, J., Spires, T., Paulson, J., Kotilinek, L., Ingelsson, M., Guimaraes, A., DeTure, M., Ramsden, M., McGowan, E., Forster, C., Yue, M., Orne, J., Janus, C., Mariash, A., Kuskowski, M., Hyman, B., Hutton, M., and Ashe, K. H. (2005) Tau suppression in a neurodegenerative mouse model improves memory function. *Science 309*, 476–481.
23. Grassetti, D. R., and Murray, J. F., Jr. (1967) The use of 2,2′-dithiodipyridine in the determination of glutathione and of triphosphopyridine nucleotide by enzymatic cycling. *Anal. Biochem. 21*, 427–434.
24. Wittekind, M., and Muller, L. (1993) HNCACB, a highly sensative 3D NMR experiment to correlate Amide-proton and nitrogen resonances with the alpha and beta-carbon resonances in proteins. *J. Magn. Reson. 101B*, 201–205.
25. Muhandiram, D., and Kay, L. (1994) Gradient-enhanced triple-resonance three-dimensional NMR experiments with improved sensitivity. *J. Magn. Reson. 103B*, 203–216.
26. Grzesiek, S., and Bax, A. (1992) *J. Magn. Reson. 99*, 201–207.
27. Kay, L. E., Ikura, M., Tschudin, R., and Bax, A. (1990) *J. Magn. Reson.* 496–514.
28. Delaglio, F., Grzesiek, S., Vuister, G. W., Zhu, G., Pfeifer, J., and Bax, A. (1995) *J. Biomol. NMR 6*, 277–293.
29. Kraulis, P. J. (1989) *J. Magn. Reson. 24*, 627–633.
30. Kraulis, P. J., Domaille, P. J., Campbell-Burk, S. L., Van Aken, T., and Laue, E. D. (1994) Solution structure and dynamics of ras p21·GDP determined by heteronuclear three- and four-dimensional NMR spectroscopy. *Biochemistry 33*, 3515–3531.
31. Kay, L. E., Torchia, D. A., and Bax, A. (1989) Backbone dynamics of proteins as studied by. *Biochemistry 28*, 8972–8979.
32. Scaramozzino, F., Peterson, D. W., Farmer, P., Gerig, J. T., Graves, D. J., and Lew, J. (2006) TMAO promotes fibrillization and

microtubule assembly activity in the C-terminal repeat region of tau. *Biochemistry 45*, 3684–3691.
33. Bai, Y., Milne, J. S., Mayne, L., and Englander, S. W. (1993) Primary structure effects on peptide group hydrogen exchange. *Proteins 17*, 75–86.
34. Wishart, D. S., and Sykes, B. D. (1994) The ^{13}C chemical-shift index: a simple method for the identification of protein secondary structure using ^{13}C chemical-shift data. *J. Biomol. NMR 4*, 171–180.
35. Wishart, D. S., Sykes, B. D., and Richards, F. M. (1992) The chemical shift index: a fast and simple method for the assignment of protein secondary structure through NMR spectroscopy. *Biochemistry 31*, 1647–1651.
36. Eliezer, D., Barre, P., Kobaslija, M., Chan, D., Li, X., and Heend, L. (2005) Residual structure in the repeat domain of tau: echoes of microtubule binding and paired helical filament formation. *Biochemistry 44*, 1026–1036.
37. Sibille, N., Sillen, A., Leroy, A., Wieruszeski, J. M., Mulloy, B., Landrieu, I., and Lippens, G. (2006) Structural impact of heparin binding to full-length Tau as studied by NMR spectroscopy. *Biochemistry 45*, 12560–12572.
38. Mukrasch, M. D., Biernat, J., von Bergen, M., Griesinger, C., Mandelkow, E., and Zweckstetter, M. (2005) Sites of tau important for aggregation populate β-structure and bind to microtubules and polyanions. *J. Biol. Chem. 280*, 24978–24986.
39. Wishart, D. S., Bigam, C. G., Holm, A., Hodges, R. S., and Sykes, B. D. (1995) ^{1}H, ^{13}C and ^{15}N random coil NMR chemical shifts of the common amino acids. I. Investigations of nearest-neighbor effects. *J. Biomol. NMR 5*, 67–81.
40. Wang, Y., and Jardetzky, O. (2002) Probability-based protein secondary structure identification using combined NMR chemical-shift data. *Protein Sci. 11*, 852–861.
41. Goux, W. J., Kopplin, L., Nguyen, A. D., Leak, K., Rutkofsky, M., Shanmuganandam, V. D., Sharma, D., Inouye, H., and Kirschner, D. A. (2004) The formation of straight and twisted filaments from short tau peptides. *J. Biol. Chem. 279*, 26868–26875.
42. Xu, S., Wu, D., Arnsdorf, M., Johnson, R., Getz, G. S., and Cabana, V. G. (2005) Chemical colloids versus biological colloids: a comparative study for the elucidation of the mechanism of protein fiber formation. *Biochemistry 44*, 5381–5389.
43. Chirita, C. N., and Kuret, J. (2004) Evidence for an intermediate in tau filament formation. *Biochemistry 43*, 1704–1714.
44. Yancey, P. H., Clark, M. E., Hand, S. C., Bowlus, R. D., and Somero, G. N. (1982) Living with water stress: evolution of osmolyte systems. *Science 217*, 1214–1222.
45. Yancey, P. H., Rhea, M. D., Kemp, K. M., and Bailey, D. M. (2004) Trimethylamine oxide, betaine and other osmolytes in deep-sea animals: depth trends and effects on enzymes under hydrostatic pressure. *Cell. Mol. Biol. 50*, 371–376.
46. Kumar, R., Lee, J. C., Bolen, D. W., and Thompson, E. B. (2001) The conformation of the glucocorticoid receptor af1/tau1 domain induced by osmolyte binds co-regulatory proteins. *J. Biol. Chem. 276*, 18146–18152.
47. Tatzelt, J., Prusiner, S. B., and Welch, W. J. (1996) Chemical chaperones interfere with the formation of scrapie prion protein. *EMBO J. 15*, 6363–6373.
48. Tamarappoo, B. K., and Verkman, A. S. (1998) Defective aquaporin-2 trafficking in nephrogenic diabetes insipidus and correction by chemical chaperones. *J. Clin. Invest. 101*, 2257–2267.
49. Brown, C. R., Hong-Brown, L. Q., Biwersi, J., Verkman, A. S., and Welch, W. J. (1996) Chemical chaperones correct the mutant phenotype of the delta F508 cystic fibrosis transmembrane conductance regulator protein. *Cell Stress Chaperones 1*, 117–125.
50. Smith, M. J., Crowther, R. A., and Goedert, M. (2000) The natural osmolyte trimethylamine N-oxide (TMAO) restores the ability of mutant tau to promote microtubule assembly. *FEBS Lett. 484*, 265–270.
51. Lippens, G., Wieruszeski, J. M., Leroy, A., Smet, C., Sillen, A., Buee, L., and Landrieu, I. (2004) Proline-directed random-coil chemical shift values as a tool for the NMR assignment of the tau phosphorylation sites. *ChemBioChem 5*, 73–78.
52. Smet, C., Leroy, A., Sillen, A., Wieruszeski, J. M., Landrieu, I., and Lippens, G. (2004) Accepting its random coil nature allows a partial NMR assignment of the neuronal Tau protein. *ChemBioChem 5*, 1639–1646.
53. Mukrasch, M. D., von Bergen, M., Biernat, J., Fischer, D., Griesinger, C., Mandelkow, E., and Zweckstetter, M. (2007) The "jaws" of the tau-microtubule interaction. *J. Biol. Chem. 282*, 12230–12239.
54. Clore, G. M., Tang, C., and Iwahara, J. (2007) Elucidating transient macromolecular interactions using paramagnetic relaxation enhancement. *Curr. Opin. Struct. Biol. 17*, 603–616.

BI702466A